Phys Chem Minerals (2006) 33:519–532
DOI 10.1007/s00269-006-0110-1

ORIGINAL PAPER

Quantum-mechanical calculation of the vibrational spectrum of beryl ($Al_4Be_6Si_{12}O_{36}$) at the Γ point

Mauro Prencipe · Yves Noel · Bartolomeo Civalleri · Carla Roetti · Roberto Dovesi

Received: 13 April 2006 / Accepted: 22 June 2006 / Published online: 19 September 2006

Abstract A quantum-mechanical calculation of the zone-centre phonon spectrum of beryl has been performed, by using an hybrid HF/DFT Hamiltonian (B3LYP). An excellent agreement with the experiment has been obtained, being the difference between the calculated and the experimental vibrational frequencies (Raman, IR-TO and IR-LO) less than 5 cm^{-1} on average. In the few cases where a relatively large disagreement between calculated and experimental data is observed, an explanation can be found which attributes the reason of the discrepancies to the experimental data rather than to the calculated ones. The calculation (i) allows the identification, in the experimental spectra, of the peaks corresponding to fundamental modes, overtones, combination bands and leakage; (ii) solves problems of band assignements due to the presence of LO–TO splitting in the IR spectra; (iii) provides the frequencies of *silent* modes; (iv) permits a full analysis of the atomic motion corresponding to each normal mode.

Keywords Vibrational spectroscopy · Quantum-mechanical calculations · Beryl

Introduction

Extensive experimental reasearch has been devoted to minerals belonging to the beryl group, whose chemical formula can be expressed as $(M^{3+},M^{2+})_4$ $[T'_6T''_{12}O_{36-z}(OH)_z]\cdot$ $(H_2O)_yA_x$ (M: octahedral cations like Al, Fe, Sc; T′ mainly Be, but also Li; T″ mainly Si; A: alkali cations like Na, K and Cs; Ferraris et al. 1998), in order to rationalise the observed correlations between structural details and crystal chemistry (Hawthorne and Cerný 1977; Aurisicchio et al. 1988; Artioli et al. 1993). The structure of beryl (ideal formula $Al_4Be_6Si_{12}O_{36}$; space group *P*6/*mcc*; see Fig. 1) consists of sixfold rings of Si-centred tetrahedra stacked along [001], interconnected by Be-centred tetrahedra and Al-centred octahedra. Al, Be and Si cations sit on the *4c*, *6f* and *12l* Wyckoff positions, respectively; 12 oxygen atoms sit on the *12l* Wyckoff position (O1), whereas the remaining 24 oxygen atoms (O2) occupy the *24m* general position. The O1 anion coordinates two Si cations and it is the shared vertex of the Si-centred tetrahedra forming the sixfold rings; O2 coordinates the Si, Al and Be cations; see Prencipe (2002) for a discussion of bonding in beryl. The stacking of the sixfold rings gives rise to channels, whose axes are parallel to [001], which can host water molecules and alkali cations. Besides X-ray and neutron diffraction

Electronic supplementary material Supplementary material is available in the online version of this article at http://dx.doi.org/10.1007/s00269-006-0110-1 and is accessible for authorized users.

M. Prencipe (✉)
Dipartimento di Scienze Mineralogiche e Petrologiche, Università di Torino, Via Valperga Caluso 35, 10125 Torino, Italy
e-mail: mauro.prencipe@unito.it

Y. Noel
Laboratoire de Pétrologie, Modélization de Matériaux et Processus, Université Pierre et Marie Curie, 4, Place Jussieu, 75232 Paris, cedex 05, France

B. Civalleri · C. Roetti · R. Dovesi
Dipartimento di Chimica IFM e NIS-Centre of excellence, Università di Torino, Via P. Giuria 7, 10125 Torino, Italy

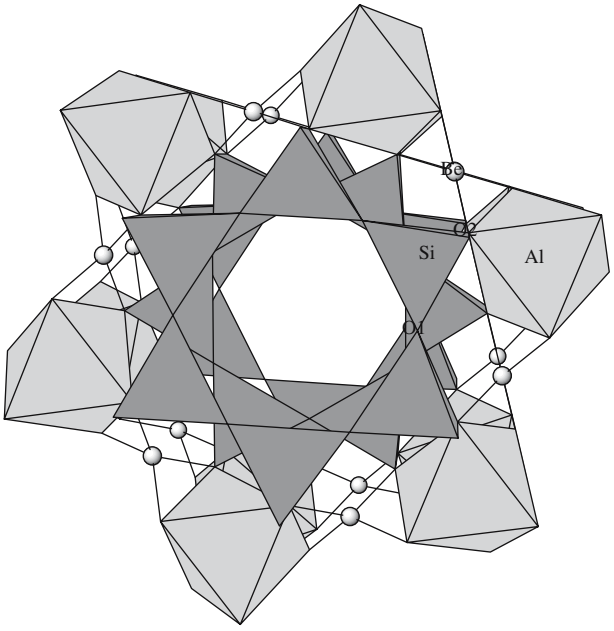

Fig. 1 Perspective view of the beryl structure, approximatively along [001]. The *dark green* polyhedra are the Si-centred tetrahedra, whereas the *light green* one's are the Al-centred octahedra; *circles* represents Be ions. The two independent oxygen atoms (O1 and O2) are shown

based studies (see for instance Artioli et al. 1993), several spectroscopic studies have been devoted to the determination of the position and orientation of the water molecule inside the channels of the structure (Wood and Nassau 1967, 1968; Aines and Rossman 1984; Hagemann et al. 1990; Charoy et al. 1996; Kolesov and Geiger 2000; Mashkovtsev et al. 2004; Gatta et al. 2006), and in a number of papers the problem of the characterization of the vibrational spectrum of *pure* beryl has been experimentally afforded (Gervais et al. 1972; Adams and Gardner 1974; Hofmeister et al. 1987; Hagemann et al. 1990; Kim et al. 1995). The identification and the characterization of the fundamental normal modes of the pure beryl is an aid in the study of isomorphous substitutions, which occurs very commonly in beryl, through the analysis of the vibrational spectra and their modifications as a function of crystal chemistry.

Kim et al. (1995) and Pilati et al. (1997) attempted the assignment of vibrational modes in beryl by using empirically determined model potentials, parametrized to reproduce observed vibrational frequencies. However this procedure is not fully satisfactory since, apart from being based on classical models of atomic interactions, requires the a priori knowledge of which modes are fundamentals and which are not; not an *easy* task.

As a contribution in the identification of fundamental frequencies and their assignement, the vibrational spectrum of beryl has been calculated ab initio, following a quantum-mechanical approach which has already been successfully applied in several cases (pyrope, Pascale et al. 2005a; andradite, Pascale et al. 2005b; katoite, Orlando et al. 2005; forsterite, Noel et al. 2006).

It should be stressed that, in general, the terms *vibrational spectrum* are used to indicate the set of frequencies of the vibrational normal modes in crystals and molecules, and *not* those functions expressing the intensity of transmission, or reflection, of the electromagnetic radiation interacting with the vibrational modes. In a crystal or molecule, atoms do vibrate independently by the interaction with the radiation used to detect and characterize such motion. As stated in the title, the aim of the paper is just the calculation and characterization of the vibrational normal modes (*phonons*) of beryl, at the Brillouin zone centre. Therefore the paper does not address the difficult problem of the interactions of those phonons with radiation in some specific experimental set up (IR and Raman spectroscopy, for example). In other words, the issue addressed in the present paper is not the reproduction or simulation of IR and Raman spectra, but the *direct* calculation of the vibrational spectrum of beryl at the Γ point. Nevertheless, in order to judge the *quality* of our results, much discussion is dedicated to the comparison of our computed frequencies with those obtained from IR and Raman spectroscopy. It must also be recognized that much of the efforts spent by the experimentalists, making IR and Raman spectroscopy, are not aimed at just obtaining *good* well resolved intensity (of radiation) versus frequencies *curves*, but at the extraction (from those curves) of the frequencies of the (active) normal modes; in doing that, especially in case of IR reflectance spectroscopy, experimentalists are often forced to use approximate models describing the interactions of radiation with matter, which are not always free of more or less arbitrary assumptions (Hawthorne and Waychunas 1988; McMillan and Hofmeister 1988). These difficulties in correctly describing the radiation-matter interaction, in order to extract the useful and relevant information from the IR and Raman spectra (that is, the frequency of vibrations) are not encountered in a *direct* calculation like the one discussed in the present paper.

The structure of the paper is as follows: a description of the method of calculation, and a discussion concerning the choice of the more critical computational parameters, is provided in the next section; a section

concerning the calculated frequencies and their comparison with the available experimental data is then provided, by separately discussing Raman and IR active normal modes. A final section is dedicated at the analysis of the atomic motions in the normal modes.

Computational details

Geometry optimization and spectra calculations were performed by means of a development version of the ab initio CRYSTAL code (Saunders et al. 2003), which implements the Hartree-Fock and Kohn-Sham, Self Consistent Field (SCF) method for the study of periodic systems (Pisani et al. 1988), by using a gaussian type basis set.

Basis set

In order to test for the variational basis dependence of the calculated frequencies, three different sets were used; the first one is similar to that used in Prencipe and Nestola (2005) for the study of beryl with different Hamiltonians, except that a second set of polarization functions have been added to Si and O. More precisely, the 66-21G(2d), 85-11G(d), 5-11G and 6-31G(2d) contractions have been used for Si, Al, Be and O respectively; in the following, this basis set will be indicated as D1. The exponents of the outer *sp* shells of the atoms were variationally optimized (Si 0.090; Al 0.466 and 0.370; Be 2.248 and 0.526; O 0.266 bohr^{-2}); the exponents of the *d* shells have been set to 2.000 and 0.510 (Si), 0.490 (Al), 2.000 and 0.500 bohr^{-2}(O).

In the second, richer, set (D2), Be was described by a 6-31G(d) contraction (Binkley and Pople 1977), where the exponents of outer *sp* and *d* shells have been reoptimized to 0.0823 and 0.4 bohr^{-2}, respectively; for Al a 88-31G(d) contraction was used as recently adopted to study α-Al_2O_3 (Montanari et al. 2006); for Si and O the basis set contained 88-31G(d) and 8-411G(d) contractions, as proposed by Nada et al. (1996). The exponents of the most diffuse functions were: α_{sp} = 0.12, α_d = 0.60 (Be); α_{sp} = 0.14, α_d = 0.51 (Al); α_{sp} = 0.193, α_d = 0.61 (Si); α_{sp} = 0.181, α_d = 0.60 bohr^{-2}) (O).

An even larger basis set (D3) was then created by simply adding a double set of *d* functions to Al, Si and O with exponents: 2.0, 0.4; 2.0, 0.5; 2.2, 0.6 bohr^{-2}, respectively.

The average of the absolute differences, $\overline{|\Delta|}$, between the frequencies calculated with the basis sets D1 and D2 is 7 cm^{-1}, whereas the same figure evaluated for the D3 and D2 basis sets reduces to 1 cm^{-1}. Thus, for accurate frequency calculations, a basis set of a quality at least comparable to D2 should be used; a further improvement of the basis quality (D3) does not produce significant changes in the results, but increases noticeably the cost of the calculation[1].

In the following, results will be presented with reference to the D3 basis set only.

Hamiltonian and computational parameters

The B3LYP Hamiltonian has been used, which contains a hybrid Hartree-Fock/Density-functional exchange-correlation term; such Hamiltonian is widely and successfully used in molecular quantum chemistry (Koch and Holthausen 2000) as well as for solid state calculations. B3LYP has already been successfully used for the calculation of the vibrational spectra of other minerals, such as α-quartz (Zicovich-Wilson et al. 2004), calcite (Prencipe et al. 2004), brucite (Pascale et al. 2004a; Ugliengo et al. 2004), pyrope (Pascale et al. 2005a). In CRYSTAL (Saunders et al. 2003), the DTF exchange-correlation functionals are evaluated by numerical integration over the cell volume. Radial and angular points of the atomic grid, at which the functionals are evaluated, are generated through Gauss-Legendre and Lebedev quadrature schemes. A grid *pruning* is usually adopted (Pascale et al. 2004b) and the influence of the grid size on both the accuracy and cost of calculation is fully discussed elsewhere (Pascale et al. 2004b, 2005a; Prencipe et al. 2004; Tosoni et al. 2005). In the present case a (75, 974) *p* grid has been used, where the notation (n_r,n_Ω)*p* indicates a pruned grid with n_r radial points and n_Ω angular points on the Lebedev surface in the most accurate integration region (see the ANGULAR keyword in the CRYSTAL user's manual, Saunders et al. 2003). Such a grid corresponds to 1583468 integration points in the unit cell. The accuracy of the integration can be measured from the error in the integrated total electron density, which amounts to $-2 \times 10^{-4}|e|$ for a total of 532 electrons.

Default values have been used for the thresholds (*ITOL1, ITOL2, ITOL3, ITOL4* and *ITOL5*) controlling the accuracy of the calculation of Coulomb and exchange integrals (Saunders et al. 2003).

The diagonalization of the Hamiltonian matrix was performed at 6 independent **k** vectors in the reciprocal space (Monkhorst net; Monkhorst and Pack 1976) by setting the shrinking factor IS (Saunders et al. 2003) to 3.

[1] The D2 and D3 basis sets are reported at the CRYSTAL web page, at the address http://www.crystal.unito.it

Geometry

Cell parameters and fractional coordinates were optimized by analytical gradient methods, as implemented in CRYSTAL (Civalleri et al. 2001; the optimization of cell parameters is implemented in the development version of the CRYSTAL code). Geometry optimization was considered converged when each component of the gradient (TOLDEG parameter in CRYSTAL) is smaller than 0.00001 hartree/bohr and displacements (TOLDEX) with respect to the previous step are smaller than 0.00004 bohr. Results (cell parameters, optimized fractional coordinates and a set of selected interatomic distances) are reported in Table 1. As usual with the B3LYP Hamiltonian (see for instance Prencipe and Nestola 2005), the cell volume is slightly overestimated (+1.8%), with respect to the experimental datum from Artioli et al. (1993). For the comparison with our geometrical data, out of the two samples refined by Artioli et al. (1993) we chosen the sample N.2 which, with respect to the sample N.1 has a composition closer to the ideal one; sample N.1 has a considerable Li content presumibly substituting Be.

Central zone phonon frequencies

The Born–Oppenheimer potential energy surface $V(\mathbf{x})$ of a system is a function of the position $\mathbf{x}$'s of the N nuclei. For a finite system, at the equilibrium nuclear configuration and within the harmonic approximation, $V(\mathbf{x})$ takes the form

$$V(\mathbf{x}) = \frac{1}{2}\sum_{ij} u_i H_{ij} u_j$$

where the i, j summations run over all the $3N$ coordinates; u_i represents a displacement of the ith cartesian coordinate from its equilibrium value; H_{ij} is the (i, j) element of the matrix of the second derivatives of the potential, evaluated at equilibrium, with respect to the displacement coordinates:

$$H_{ij} = \frac{1}{2}\left[\frac{\partial^2 V(\mathbf{x})}{\partial u_i \partial u_j}\right]_0$$

Phonon frequencies are then evaluated as the eigenvalues of the weighted Hessian matrix W, whose (i, j) element is defined as $W_{ij} = H_{ij}/\sqrt{M_i M_j}$, where M_i and M_j are the masses of the atoms associated with the i and j coordinates, respectively.

In periodic systems, the W matrix can be given a block-diagonal form, each block being associated with a different $\mathbf{q}$-point in the first Brillouin zone [$W(\mathbf{q})$]. The $\mathbf{q} = \mathbf{0}$ point (Γ point) is of special importance, because IR and RAMAN spectra refer to this point. Central zone ($\mathbf{q} = \mathbf{0}$) phonon frequencies are the eigenvalues of the $W(\mathbf{0})$ matrix:

$$W_{ij}(\mathbf{0}) = \sum_{\mathbf{G}} \frac{H_{ij}^{\mathbf{0G}}}{\sqrt{M_i M_j}}$$

where $H_{ij}^{\mathbf{0G}}$ is the second derivative of $V(\mathbf{x})$, at equilibrium, with respect to atom i in cell $\mathbf{0}$ (translation invariance is exploited) and atom j in cell $\mathbf{G}$. By the way, once the Hessian matrix H is calculated, frequency shifts due to isotopic substitutions can readibly be calculated, at no cost, by accordingly changing the masses M_i, in the above formula. In the present case, isotopic effects have been estimated in the cases of substitution of ^{10}Be for ^{9}Be, ^{30}Si for ^{28}Si and ^{18}O for ^{16}O; such isotopes were chosen accordingly to a natural abundance criterium (second in abundance). In the case of Al, isotopic effect was estimated with the substitution of ^{29}Al for ^{27}Al, which however has a zero natural abundance (^{27}Al has a natural abundance of 100%).

The energy first derivatives with respect to the atomic positions, $v_j = \partial V/\partial u_j$, are calculated analytically (Doll et al. 2001) for all u_j coordinates. Second derivatives at $\mathbf{u} = \mathbf{0}$ were calculated numerically using the formula:

Table 1 Calculated (Calc) and experimental (Exp, Artioli et al. 1993) structural data of beryl

	Calc	Exp
a	9.2775	9.218(2)
c	9.2409	9.197(2)
V_o	688.82	676.8(4)
Si		
x	0.3871	0.3872
y	0.1151	0.1157
O1		
x	0.3089	0.3098
y	0.2352	0.2363
O2		
x	0.4985	0.4987
y	0.1448	0.1454
z	0.1455	0.1452
S–O1*a*	1.6053	1.593(2)
S–O1*b*	1.6079	1.597(2)
S–O2 (×2)	1.6329	1.622(1)
Be–O2 (×4)	1.6605	1.656(1)
Al-O2 (×6)	1.9228	1.909(1)

Lattice constants (*a* and *c*) and interatomic distances are in Å; cell volume (V_o) is in Å^3 ; *x*, *y* and *z* are fractional coordinates. Errors on the experimental data, on the last digit, are given in *parentheses*; the errors on the experimental fractional coordinates are of the order of 1×10^{-4}

$$\left[\frac{v_j}{u_i}\right]_0 \approx \frac{v_j(0,\cdots,u_i,\cdots) - v_j(0,\cdots,0,\cdots)}{u_i}$$

where the magnitude of the displacement u_i of each atomic coordinate was set to $u = 0.001$. Such formula was proved to be accurate in previous works (Pascale et al. 2005a; Zicovich-Wilson et al. 2004).

In principle, since the number of atoms (N) in the unit cell is 58, a total of $3N + 1 = 175$ energy and gradient calculations should be performed. However in CRYSTAL the point symmetry of the system (6/*mmm* in the present case) is fully exploited, so that only 14 SCF + gradient calculations were required. Another point is that, in the CRYSTAL code, the hessian matrix is block diagonalized by symmetry, so that modes are automatically symmetry classified.

Since the energy variations for the displacements here considered can be as small as 10^{-6} *to* 10^{-7} hartree, the tolerance on the convergence of the SCF cycles has been set to 10^{-9} hartree.

In the case of ionic compounds, a correction must be added to the Hessian in order to obtain the TO–LO splitting. Such a correction takes into account long range Coulomb effects due to coherent displacement of the crystal nuclei (see Born and Huang 1954, Sects. 5, 10, 34, 35; see also Umari et al. 2001) and depends essentially on the electronic (clamped nuclei) dielectric tensor ϵ^{∞} and on the *Born effective charge tensor* associated with each atom. In the present case, the latter is evaluated through well localized Wannier functions (Baranek et al. 2001; Zicovich-Wilson et al. 2001, 2002; Noel et al. 2002), whereas the former is from experimental data ($\epsilon_{xx} = 2.4618$, $\epsilon_{zz} = 2.4492$; Deer et al. 1992).

Results and discussion

There are 58 atoms in the unit cell, giving rise to 174 vibrational modes. Their symmetry decomposition corresponds to:

$$\Gamma_{\text{tot}} = 7A_{1g} + 9A_{2g} + 7B_{1g} + 6B_{2g} + 13E_{1g} + 16E_{2g} + 5A_{1u} + 7A_{2u} + 9B_{1u} + 8B_{2u} + 17E_{1u} + 12E_{2u}$$

Three modes ($A_{2u} + E_{1u}$) correspond to rigid translations of the whole crystal; 38 modes ($6A_{2u} + 16E_{1u}$) are IR active; 65 modes ($7A_{1g} + 13E_{1g} + 16E_{2g}$) are Raman active and the remaining 68 modes ($9A_{2g} + 7B_{1g} + 6B_{2g} + 5A_{1u} + 9B_{1u} + 8B_{2u} + 12E_{2u}$) are inactive (silent modes).

Frequency of the normal modes: Raman

Three sets of experimental data are available for the RAMAN active modes, due to Kim et al. (1995), Hagemann et al. (1990) and Adams and Gardner (1974) (to be indicated in the following as Exp1, Exp2, Exp3). One of the factors that influence to some extent the experimental spectra is the purity of the sample. Hagemann et al. (1990) (Exp2 data set) reported the Raman frequencies measured on beryl crystals having different composition. In particular, Beryl A is a synthetic sample which contains Cr_2O_3 (0.73 wt%) and a minor amount of other impurities; Beryl B, C and D contain Fe, as well as alkali cations and water (see Table 1 in Hagemann et al. 1990). Since Hagemann et al. (1990) considered sample A to be the most representative of *pure beryl* among the samples they analysed, the corresponding experimental data set (see Table 2 in Hagemann et al. 1990) is here considered for the comparison with the calculated spectrum. Kim et al. (1995) and Adam and Gardner (1974) used natural beryl crystals to collect their data, but did not make any comment concerning the purity of the samples.

The three sets of experimental data are reported with the present calculated ones in Table 2. It must be noticed that in the table there are 10, 16 and 19 lines for A_{1g}, E_{1g} and E_{2g}, respectively, in spite of the fact that there are only 7, 13 and 16 active modes for the three symmetries; the 3 extra lines for each symmetry contain peaks which are experimentally observed at frequencies with no calculated counterpart, and vice-versa.

Apart from these specific cases, to which we will come back later on, there is, in general, a fairly good agreement between the four sets of Table 2, as documented by Table 3, where four statistical indices are reported, that are defined as follows (with reference to two data sets a and b): $\overline{\Delta\omega} = \sum_i^N (\omega_i^a - \omega_i^b)/N$; $\overline{|\Delta\omega|} = \sum_i^N |\omega_i^a - \omega_i^b|/N$; $(\Delta\omega)_{\min}$ and $(\Delta\omega)_{\max}$ are respectively the minimum and maximum values in the set $\{\omega_i^a - \omega_i^b\}_{i=1,N}$, where N is the number of data given in the first line of Table 3. N is always smaller than the total number of expected peaks (36) because, obviously, in some of the lines of Table 2 one of the two numbers to be compared is lacking. It is however interesting to note that when 32, 31 or 33 peaks out of 36 are included in the statistics, the experimental sets agree among them extremely well, with a mean absolute difference of 2–3 cm^{-1}, and a maximum difference of 14 cm^{-1}.

Such an extremely good agreement also exists between the calculated and the experimental data, with

Table 2 Calculated (Calc) and experimental (Exp1, Exp2 and Exp3) frequencies (v, in cm^{-1}) of the Raman active modes

	Calc	Exp1		Exp2		Exp3	
	v	v	Δ	v	Δ	v	Δ
A_{1g}							
1	–	–		–		214	
2	–	240		240		–	
3	272	–		–		–	
4	324	323	+1	320	+4	324	0
5	395	396	–1	394	+1	396	–1
6	630	625	+5	623	+7	626	+4
7	692	685	+7	682	+10	686	+6
8	1,065	1,070	–5	1,066	–1	1,068	–3
9	1,132	1,139	–7	1,139	–7	1,125	+7
10	–	1,192		–		–	
$\overline{\lvert\Delta\rvert}$			4		5		4
E_{1g}							
11	–	59		–		–	
12	138	–		140	–2	131	+7
13	145	144	–1	146	–1	145	0
14	197	192	+5	192	+5	188	+9
15	253	255	–2	253	0	254	–1
16	296	298	–2	296	0	297	–1
17	386	382	+4	381	+5	383	+3
18	446	450	–4	449	–3	450	–4
19	453	–		–		–	
20	524	529	–5	527	–3	529	–5
21	672	683	–11	683	–11	683	–11
22	771	771	0	769	+2	770	+1
23	907	919	–12	919	–12	918	–11
24	1,007	1,014	–7	1,010	–3	1,012	–5
25	–	1,070		–		–	
26	–	1,221		–		–	
$\overline{\lvert\Delta\rvert}$			5		4		5
E_{2g}							
27	146	146	0	144	+2	146	0
28	184	185	–1	184	0	187	–3
29	–	222		–		–	
30	287	291	–4	288	–1	291	–4
31	314	322	–8	315	–1	318	–4
32	359	–		–		–	
33	–	398		396		397	
34	422	423	–1	421	+1	424	–2
35	444	444	0	443	+1	444	0
36	566	565	+1	562	+4	565	+1
37	579	584	–5	581	–2	583	–4
38	682	685	–3	683	–1	685	–3
39	748	–		–		–	
40	776	772	+4	770	+6	772	+4
41	905	914	–9	916	–9	914	–9
42	997	1,004	–7	1,006	–9	1,005	–8
43	–	1,071		–		–	
44	1,228	1,230	–2	1,229	–1	1,225	+3
45	1,247	1,245	+2	1,243	+4	1,243	+4
$\overline{\lvert\Delta\rvert}$			3		3		4

$\Delta = v_{calc} - v_{exp}$; $\overline{\lvert\Delta\rvert}$ is the average over the absolute Δ values. Exp1, Exp2 and Exp3 data sets are respectively from Kim et al. (1995), Hagemann et al. (1990) and Adams and Gardner (1974)

a mean absolute error of only 4 cm^{-1} and a maximum difference of 10 cm^{-1}. This good agreement refers to 30, 32 and 32 frequencies out of 36.

We can now pass to discuss the remaining cases (6, 4 and 4 when comparing our calculated data with Exp1, 2 and 3), where large differences are observed.

Table 3 Average difference ($\overline{\Delta}$), average absolute difference ($\overline{|\Delta|}$), minimum (Δ_{min}) and maximum (Δ_{max}) differences (in cm^{-1}) among calculated and experimental data

	Exp1	Exp2	Exp3
Calc			
N	30	32	32
$\overline{\Delta}$	–2	–1	–1
$\overline{\lvert\Delta\rvert}$	4	4	4
Δ_{min}	–12	–12	–11
Δ_{max}	7	10	9
Exp1			
N		32	31
$\overline{\Delta}$		2	1
$\overline{\lvert\Delta\rvert}$		2	2
Δ_{min}		–2	–2
Δ_{max}		7	14
Exp2			
N			33
$\overline{\Delta}$			0
$\overline{\lvert\Delta\rvert}$			3
Δ_{min}			–4
Δ_{max}			14

N is the number of lines used in the calculation of the averages (see text for explanation)

We can classify these cases in three classes:

1. Calculated frequencies which are not observed in any experimental data set (lines 3, 19, 32 and 39).
2. Calculated frequencies which are not observed in only one of the experimental data set (line 12).
3. Experimental peaks which do not correspond to any calculated frequency (lines 1, 2, 10, 11, 25, 26, 29, 33 and 43).

Since at the moment we are unable to compute the intensities of the Raman signals, we cannot prove that the calculated frequencies belonging to the first group are not observed experimentally because of their very low intensity; however this is the most likely explanation.

Mode at line 12 is the only one belonging to the second group. Kim et al. (1995) did not identify such mode in their spectrum and they explained its occurrence in the spectra of other Authors (Hagemann et al. 1990; Adams and Gardner 1974) as due to the presence of lattice defects. On the basis of our calculation, we think that such peak corresponds to a fundamental vibrational mode.

Several peaks belong to the third group. Let us consider first lines 1, 2 and 3. In Kim et al. (1995), the lowest frequency reported for the A_{1g} symmetry is at 240 cm^{-1}. However, visual inspection of the spectra reported by these authors (see Fig. 2 in Kim et al. 1995) shows that a very weak absorption (which is hardly distinguishable from the background) is present at that frequency. Hagemann et al. (1990) did not report such frequency for beryl C, and only a very weak absorption is observed for Beryl A (see Fig. 1a in Hagemann et al. 1990). Adams and Gardner (1974) reported a weak (but visible) and broad absorption band around 214 cm^{-1}, but no peak at 240 cm^{-1}. Hagemann et al. (1990) concluded that the position of such peak may depend on the presence of impurities in the structure of beryl. It should be noted that alkali cations, if sitting at the 2*a* or 2*b* Wyckoff positions (as generally assumed) should not contribute to A_{1g} modes; however, as discussed in Prencipe (2002), the positions they actually occupy are probably off the [001] sixfold symmetry axis of the channel (on which are located the two 2*a* and 2*b* Wyckoff positions) and in this case they could contribute to normal modes with that symmetry (by the way, it is also to be noted that, if disorder is present in the positions of cations in the channel, on average the sixfold symmetry axis is preserved, and the possible displacements of cations off [001] cannot be detected by diffraction techniques). Moreover, even if Al and Be should not directly contribute to the A_{1g} modes, they are bound to oxygens (O2) which do contribute to those modes; therefore the substitution of some Al with Cr [as in the case of beryl A, in Hagemann et al. (1990)] could in general have an influence on the observed frequencies.

The lowest calculated A_{1g} frequency is at 272 cm^{-1}. It is stressed that in the calculated spectrum, at variance with experiment, there is no reason for large errors on a few, out of many, individual frequencies, as all the frequencies are generated by the same algorithm and are then affected, roughly speaking, by the same error (due to the selected Hamiltonian, limitations in the basis set, numerical errors); therefore we believe that our calculated datum corresponds to the frequency of a fundamental A_{1g} normal mode of pure beryl, which is not experimentally observed possibly because of its low intensity. Very weak signals (if any) at lower frequencies, in the experimental spectra, could be due to the presence of impurities in the samples.

Let us consider now line 10. At variance with respect to Hagemann et al. (1990) and Adams and Gardner (1974), Kim et al. (1995) reported a very weak A_{1g} peak at 1,192 cm^{-1} (line 10). On the basis of our calculation, we propose that this peak (which is indeed invisible in the published spectrum: see Fig 2 in Kim et al. 1995) is an overtone. It is to be noted that, having reached the maximum number of fundamental A_{1g} modes (7), Kim et al. (1995) were forced to assign to an overtone another observed peak (mode 9, at 1,139 cm^{-1}). Their interpretation of the nature of this

peak is not confirmed by Hagemann et al. (1990) and Adams and Gardner (1974); our calculation gives a fundamental A_{1g} mode at 1,132 cm^{-1}, that is very close to their supposed *overtone*.

The situation is similar for lines 11 and 12: Kim et al. (1995) reported an E_{1g} mode at 59 cm^{-1} (line 11) which, judging from a visual inspection of their spectrum (Fig. 2 in Kim et al. 1995), is very hardly distinguishable from background noise. No peak was reported in this region by the two other experimental groups or results from our calculation.

The E_{1g} peak observed at 683 cm^{-1} (line 21) was attributed by the three Authors to leakage, due to sample misorientation with respect to the incident and scattered light polarizations. Indeed, strong absorptions were observed at about the same frequency in the A_{1g} and E_{2g} experimental spectra (lines 7 and 38). For this reason, these Authors did not assign the peak at 683 cm^{-1} to any fundamental E_{1g} mode. However, a E_{1g} mode is calculated at 672 cm^{-1}, which is quite close to the experimental frequency at 683 cm^{-1}. The observed peak might then not be due to leakage. As we cannot evaluate its intensity, the hypothesis of leakage for the experimental peak at 683 cm^{-1} should be supplemented by that of a very low intensity of the calculated peak at 672 cm^{-1}. Alternatively we can suppose that the observed peak at 683 cm^{-1} corresponds to the calculated one at 672 cm^{-1}, and then that it is a fundamental peak.

Another possible leakage was proposed by Adams and Gardner (1974) and Hagemann et al. (1990), who did not report E_{1g} modes at frequencies higher than about 1,010 cm^{-1}, even if a peak close to 1,070 cm^{-1} is clearly observed in their E_{1g} spectra, because a very strong A_{1g} peak is observed at the same frequency; for the same reason, a E_{2g} peak observed at 1,070 cm^{-1} is not reported. Consistently with their analysis, our calculations do not provide any E_{1g} or E_{2g} mode with a frequency close to that of the A_{1g} mode calculated at 1,065 cm^{-1}. Kim et al. (1995), who invoked leakage to explain the presence of the E_{1g} peak at 683 cm^{-1}, did not use the same argument to justify the presence in their E_{1g} and E_{2g} spectra of peaks at just 1,070 cm^{-1}, which were attributed to some fundamental mode in their analysis.

Moving now to the E_{2g} spectrum, apart from a peak observed only by Kim et al. (1995) at 222 cm^{-1} (line 29 in Table 2), the largest discrepancy with our calculated data, which fall under the third group of the above classification, is the mode at line 33 reported in all the experimental papers at about 397 cm^{-1}. The closest calculated mode is 40 cm^{-1} apart, too far for invoking inaccuracies in our model. The observed modes can possibly be explained by invoking, once more, leakage from the A_{1g} spectrum (an intense A_{1g} is present at 396 cm^{-1}): the leakage from A_{1g} in E_{2g} is confirmed by the peak at 1,071 cm^{-1} reported by Kim et al. (1995) (line 43, unobserved by Hagemann et al. 1990; and by Adams and Gardner 1974).

Frequency of the normal modes: infrared

Several sets of experimental frequencies of the infrared active modes, are available. Data sets may differ in the method used to collect the spectra (single crystal reflectance, single crystal transmission, powder spectra) and in their interpretation (in the case of single crystal reflectance, the position of the band can be either directly estimated by visual inspection of the spectrum, or by fitting methods making use of the Kramer–Krönig relation; McMillan and Hofmeister 1988). In the case of single crystal transmission, the TO modes should be observed only, provided the crystal is thin enough; however a *contamination* from the LO component can be expected (McMillan and Hofmeister 1988), leading to a shift of the observed TO frequencies at higher values. Single crystal reflectance spectra should provide both TO and LO modes, but the procedure required to extract the relevant information is not always straightfoward and might lead to uncertainties in the retrieved data. Bands in powder spectra are, in general, superposition of absorption from both TO and LO modes, with weights depending upon the distribution of particle size and orientation (see *e.g.* McMillan and Hofmeister 1988).

Table 4 (TO modes) and 5 (LO modes) report experimental data from Gervais et al. (1972; Exp1), Adams and Gardner (1974; Exp2) and Hofmeister et al. (1987; Exp3). Exp1 and Exp2 data sets are from single crystal reflectance spectra; in both cases frequencies of the modes, shown in Tables 4 and 5, were determined by fitting methods through the Kramer–Krönig relation, but in the case of A_{2u} modes in Adams and Gardner (1974) (Exp2; the Authors claimed it was impossible to properly fit the reflectance spectrum). Adams and Gardner (1974), also reported the E_{1u} frequencies determined by visual inspection of the spectrum; the average absolute differences ($\overline{|\Delta|}$) of such frequencies with respect to those determined by the fitting method being 7 (TO) and 5 cm^{-1} (LO). These figures could be taken as a measure of the uncertainty associated with the measurement of the experimental frequencies. A slightly larger difference exists between the Exp1 and Exp2 data sets ($\overline{|\Delta|} =$ 8 cm^{-1}, calculated over the E_{1u} fitted frequencies). The Exp3 columns in Tables 4 and 5 (Hofmeister et al.

Table 4 Calculated (Calc) and experimental (Exp1, Exp2 and Exp3) frequencies (v, in cm^{-1}) of the infrared active TO modes

	Calc		Exp1		Exp2		Exp3	
	v	Intensity	v	Δ	v	Δ	v	Δ
A_{2u}(TO)								
1	207	120	–		201	+6	207	0
2	359	1,556	362	–3	364	–5	368	–9
3	422	1,983	423	–1	419	+3	425	–3
4	532	182	537	–5	532	0	538	–6
5	735	3,467	733	+2	734	+1	743	–8
6	905	9,075	916	–11	924	–19	–	
$\overline{\lvert\Delta\rvert}$				4		6		5
E_{1u}(TO)								
7	186	1	–		–		–	
8	256	337	–		252	+4	258	–2
9	309	3	–		–		–	
10	348	111	350	–2	342	+6	349	–1
11	377	173	–		376	+1	373	+4
12	386	140	382	+4	–		–	
13	484	8,068	488	–4	492	–8	482	+2
14	512	2,064	517	–5	528	–16	–	
15	590	953	588	+2	596	–6	590	0
16	654	382	652	+2	656	–2	653	+1
17	682	2,316	674	+8	682	0	691	–9
18	807	3,700	803	+4	796	+11	–	
19	954	6,600	955	–1	958	–4	953	+1
20	1,012	640	1,016	–4	1,014	–2	1,019	–7
21	1,184	165	–		–		–	
22	1,194	9,464	1,196	–2	1,200	–6	1,185	+9
$\overline{\lvert\Delta\rvert}$				3		5		4

$\Delta = v_{calc} - v_{exp}$; $\overline{|\Delta|}$ is the average over the absolute Δ values. Exp1, Exp2 and Exp3 data sets are respectively from Gervais et al. (1972), Adams and Gardner (1974) and Hofmeister et al. (1987)

1987) are from powder and single crystal transmission spectra; according to the Authors, the powder spectrum should record mainly TO modes, eventually shifted at higher frequencies due to the presence of LO components; the single crystal spectrum contains lines at frequencies close to those found in the spectrum of the powder (assigned to TO modes), plus a number of peaks not seen in the latter spectrum and assigned to LO modes.

Let us now consider the comparison with our calculated data in the case of TO modes. Out of a total of 22 infrared active modes, 10 calculated frequencies were not observed in at least one of the experimental data sets (modes 1, 6, 7–9, 11, 12, 14, 18 and 21) whereas no frequency has been experimentally observed, with no calculated counterpart. In all but a few cases (modes 6, 14 and 18, which were not reported by Hofmeister et al. 1987, only) the experimentally unobserved frequencies correspond to modes having a very low calculated intensity; this is likely to be the reason they were not experimentally observed. The largest discrepancies between calculated and experimental data (Exp2 data set) concern lines 6 and 14 only, and are however smaller than 20 cm^{-1} (differences with respect to Exp1 are significantly smaller).

In the case of LO modes, a significant number of lines were not experimentally observed, presumibly due to their low, or very low, intensities (Table 5, modes 1, 4, 7–12, 16, 21). Several strong lines were not reported by Hofmeister et al. (1987; Exp3) probably because, as written above, the technique they used to collect the spectrum (single crystal transmission) is not suitable to record LO modes; moreover the frequencies assigned to LO modes could be underestimated as an effect of contamination from the TO component. In fact, the largest discrepancies with our calculated data concern the Exp3 set, with the experimental LO frequencies being lower than the calculated ones, apart the case of line 16 which has, however, also a low intensity. It is to be stressed that the relatively high disagreement between the calculated and the Exp3 data sets is observed in the case of the LO modes only, consistently with the discussion above.

At variance with Gervais et al. (1972) and Adams and Gardner (1974), Hofmeister et al. (1987) attributed the E_{1u} line at 1,279 cm^{-1} to a fundamental TO mode; in their reasoning, such a peak has a too high

Table 5 Calculated (Calc) and experimental (Exp1, Exp2 and Exp3) frequencies (v, in cm^{-1}) of the infrared active LO modes

	Calc		Exp1		Exp2		Exp3	
	v	Intensity	v	Δ	v	Δ	v	Δ
A_{2u}(LO)								
1	210	19	–		210	0	–	
2	376	104	375	+1	376	0	–	
3	472	838	473	–1	484	–12	470	+2
4	538	146	–		554	–16	–	
5	771	804	771	0	772	–1	–	
6	1,093	14,435	1,100	–7	1,100	–7	–	
$\overline{\lvert\Delta\rvert}$				2		6		
E_{1u}(LO)								
7	186	0	–		–		–	
8	260	55	–		262	+2	–	
9	309	1	–		–		–	
10	349	12	–		350	–1	–	
11	378	12	–		–		–	
12	387	18	–		387	0	–	
13	504	84	502	+2	510	–6	–	
14	561	1,471	560	+1	564	–3	557	+4
15	606	1,211	608	–2	615	–9	602	+4
16	656	131	–		660	–4	668	–12
17	707	1,869	703	+4	706	+1	–	
18	836	2,344	825	+11	836	0	823	+13
19	997	2,429	995	+2	1,002	–5	978	+19
20	1,029	4,650	–		1,032	–3	–	
21	1,184	4	–		–		–	
22	1,285	21,142	1,283	+2	1,290	–5	1,279	+6
$\overline{\lvert\Delta\rvert}$				3		3		10

See caption to Table 4 for explanation

intensity to be attributed to an LO mode coupled with a TO mode (the one at 1,185 cm^{-1}, line 22 in Table 4) having much lower intensity. However in our calculation we found an LO mode at 1,285 cm^{-1} (line 22 in Table 5) whose intensity is more than twice the intensity of the coupled TO mode calculated at 1,194 cm^{-1} (line 22 in Table 4). Therefore, in agreement with Gervais et al. (1972) and Adams and Gardner (1974), we propose that the peak observed by Hofmeister et al. (1987) at 1,279 cm^{-1} is indeed an LO mode.

Analysis of the normal modes

Vibrational modes in silicates are usually classified either as *internal* (*I*; stretching or bending modes of the covalent polyhedra, namely the SiO_4 tetrahedra) or *external* (*E*; modes involving the motion of other cations and rotations and translations of the tetrahedra). This classification, however, tends to greatly simplify the reality and, in general, neither *pure I* nor *E* modes can be identified.

Ab initio calculations provide several tools for the analysis of the nature of the relative motion of atoms in a given normal mode: (i) direct inspection of the eigenvectors of the dynamical matrix; (ii) isotopic substitution of species in the unit cell: a zero (small) frequency shift indicates that the substituted atom does not move; (iii) graphical representation of the eigenvectors. These tools have already been successfully applied in the study of pyrope (Pascale et al. 2005a), andradite (Pascale et al. 2005b), katoite (Orlando et al. 2005) and forsterite (Noel et al. 2006).

Eigenvectors are deposited and they are available upon request. Isotopic shifts, referring to the present system, are reported in Table 6: normal modes are ranked according to their frequency (independently by their symmetry), and the label attributed to each mode is, in general, different from that given in Tables 2, 4 or 5. Figure 2(a–d) shows graphically the magnitude of the isotopic shift effects on the different atoms. As shown in Fig. 2a, Be mainly participates to modes in the range between 590 and 880 cm^{-1} with isotopic shifts larger than 14 cm^{-1}. By considering, for instance, Raman and IR active normal modes only, it appears that Be is involved in (i) modes 41, 76 and 84 of E_{1g} symmetry; (ii) E_{2g} modes 38, 67, 77, and 85; (iii) A_{2u} modes 46 and 81; (iv) the E_{1u} modes 40, 69, 75, 78, 88. Al is in a special position and octahedrally coordinated. It gives small shifts mainly affecting low frequency modes

Table 6 Effect of the ^{10}Be, ^{29}Al, ^{30}Si and ^{18}O isotopic substitutions on the calculated wavenumbers v (cm^{-1}) of all modes

n		v	Δv				n		v	Δv			
			^{10}Be	^{29}Al	^{30}Si	^{18}O				^{10}Be	^{29}Al	^{30}Si	^{18}O
1	B_{1g}	135	0	1	0	**6**	58	E_{2u}	509	0	0	**5**	**22**
2	E_{1g}	138	0	0	1	**6**	59	E_{1u}	512	1	**2**	**3**	**21**
3	E_{1g}	145	0	0	0	**8**	60	B_{1u}	519	**8**	0	**2**	**19**
4	E_{2g}	146	0	0	1	**6**	61	E_{1g}	524	1	**2**	**5**	**15**
5	E_{2u}	150	1	0	1	**7**	62	A_{2g}	526	**10**	0	**3**	**14**
6	B_{1u}	172	0	0	0	**9**	63	A_{2u}	533	0	1	1	**28**
7	E_{2g}	184	0	0	1	**9**	64	E_{2u}	544	0	0	**2**	**26**
8	E_{1u}	186	0	0	**2**	**7**	65	E_{2g}	566	0	0	**4**	**26**
9	E_{2u}	186	0	0	0	**10**	66	A_{1u}	566	0	0	**6**	**23**
10	B_{2u}	193	0	0	0	**11**	67	E_{2g}	579	**8**	**4**	**4**	**14**
11	E_{1g}	197	1	**2**	0	**8**	68	A_{2g}	583	0	0	**3**	**28**
12	A_{2u}	207	0	0	0	**11**	69	E_{1u}	590	**14**	0	**4**	**14**
13	B_{1g}	215	0	1	1	**9**	70	A_{1u}	599	0	0	1	**32**
14	B_{2g}	219	0	0	0	**12**	71	E_{2u}	601	**2**	**4**	1	**22**
15	B_{1u}	219	1	0	**2**	**8**	72	A_{1g}	630	0	0	**3**	**32**
16	A_{1u}	220	0	0	1	**11**	73	B_{1u}	641	**17**	**2**	**4**	**7**
17	E_{2u}	223	0	0	0	**12**	74	B_{1g}	650	**21**	1	**3**	**6**
18	A_{2g}	231	0	0	**5**	**5**	75	E_{1u}	654	**4**	0	**13**	**13**
19	E_{1g}	253	0	1	1	**12**	76	E_{1g}	672	**21**	0	**2**	**10**
20	E_{1u}	256	1	**2**	1	**10**	77	E_{2g}	682	**15**	**2**	**4**	**12**
21	E_{2u}	264	0	0	1	**14**	78	E_{1u}	682	**9**	1	**11**	**8**
22	A_{1g}	272	0	0	**7**	**5**	79	E_{2u}	691	**24**	1	**3**	**6**
23	B_{2g}	278	0	0	1	**15**	80	A_{1g}	692	0	0	**12**	**20**
24	E_{2g}	287	0	**2**	**2**	**12**	81	A_{2u}	734	**24**	**2**	**2**	**8**
25	A_{2g}	296	0	1	**2**	**12**	82	B_{2u}	743	**11**	0	**19**	1
26	E_{1g}	296	0	1	**2**	**12**	83	E_{2g}	748	0	0	**17**	**14**
27	B_{1g}	299	**2**	**2**	**2**	**10**	84	E_{1g}	771	**28**	**2**	0	**8**
28	B_{2u}	301	0	0	**4**	**12**	85	E_{2g}	776	**3**	0	**18**	**10**
29	B_{1u}	306	0	**6**	1	**6**	86	B_{2g}	782	**28**	0	0	**13**
30	E_{1u}	309	0	0	**2**	**13**	87	B_{1u}	803	0	0	**24**	**5**
31	E_{2g}	314	0	0	**2**	**16**	88	E_{1u}	807	**27**	**2**	**3**	**7**
32	A_{1u}	322	0	0	**2**	**15**	89	A_{2g}	818	**15**	**2**	**12**	**6**
33	A_{1g}	324	0	0	**2**	**15**	90	B_{1u}	869	1	0	**5**	**40**
34	A_{2g}	337	0	**3**	0	**15**	91	B_{2u}	879	**16**	0	**7**	**18**
35	E_{2u}	342	0	**7**	1	**7**	92	B_{1g}	902	0	0	**13**	**29**
36	E_{1u}	348	0	0	0	**20**	93	E_{2u}	903	0	0	**12**	**29**
37	A_{2u}	359	1	**9**	0	**5**	94	A_{2u}	905	0	0	**13**	**27**
38	E_{2g}	359	**2**	**2**	**3**	**11**	95	E_{2g}	905	1	0	**8**	**33**
39	E_{1u}	378	1	**4**	**5**	**12**	96	E_{1g}	907	0	0	**13**	**30**
40	E_{1u}	386	**4**	1	1	**13**	97	E_{1u}	954	**2**	0	**10**	**33**
41	E_{1g}	386	**7**	0	1	**14**	98	E_{2g}	997	0	0	**6**	**46**
42	A_{2g}	393	**2**	**6**	0	**8**	99	B_{2u}	1006	**2**	0	**3**	**49**
43	A_{1g}	395	0	0	0	**22**	100	E_{1g}	1007	1	0	**9**	**40**
44	B_{2g}	416	**5**	0	**2**	**17**	101	E_{1u}	1012	0	0	**8**	**43**
45	E_{2u}	420	**3**	1	**4**	**13**	102	A_{2g}	1018	**6**	1	**5**	**38**
46	A_{2u}	422	**4**	0	**2**	**16**	103	E_{2u}	1042	0	0	**10**	**41**
47	E_{2g}	422	1	**6**	0	**13**	104	A_{1g}	1065	0	0	**9**	**44**
48	B_{1g}	429	**4**	**8**	**2**	**4**	105	B_{2g}	1072	**3**	0	**10**	**39**
49	B_{2u}	433	**3**	0	**2**	**19**	106	A_{1u}	1131	0	0	**13**	**42**
50	E_{2g}	444	0	0	**5**	**16**	107	A_{2g}	1132	0	0	**8**	**50**
51	E_{1g}	446	1	**5**	**3**	**15**	108	A_{1g}	1132	0	0	**8**	**50**
52	E_{1g}	453	1	0	1	**20**	109	E_{1u}	1184	0	0	**8**	**54**
53	B_{1u}	459	1	**5**	**2**	**14**	110	E_{1u}	1194	1	0	**8**	**53**
54	B_{2u}	461	**3**	0	**5**	**15**	111	B_{1u}	1226	0	0	**5**	**60**
55	E_{1u}	484	0	**3**	**3**	**18**	112	E_{2g}	1228	1	0	**7**	**57**
56	B_{2g}	490	0	0	**9**	**13**	113	E_{2g}	1247	0	0	**8**	**57**
57	B_{1g}	507	0	0	0	**28**	114	B_{2u}	1256	**3**	0	**7**	**56**

Isotopic shifts larger than 2.0 cm^{-1} are in bold-type. Vibrational frequencies reported in increasing order

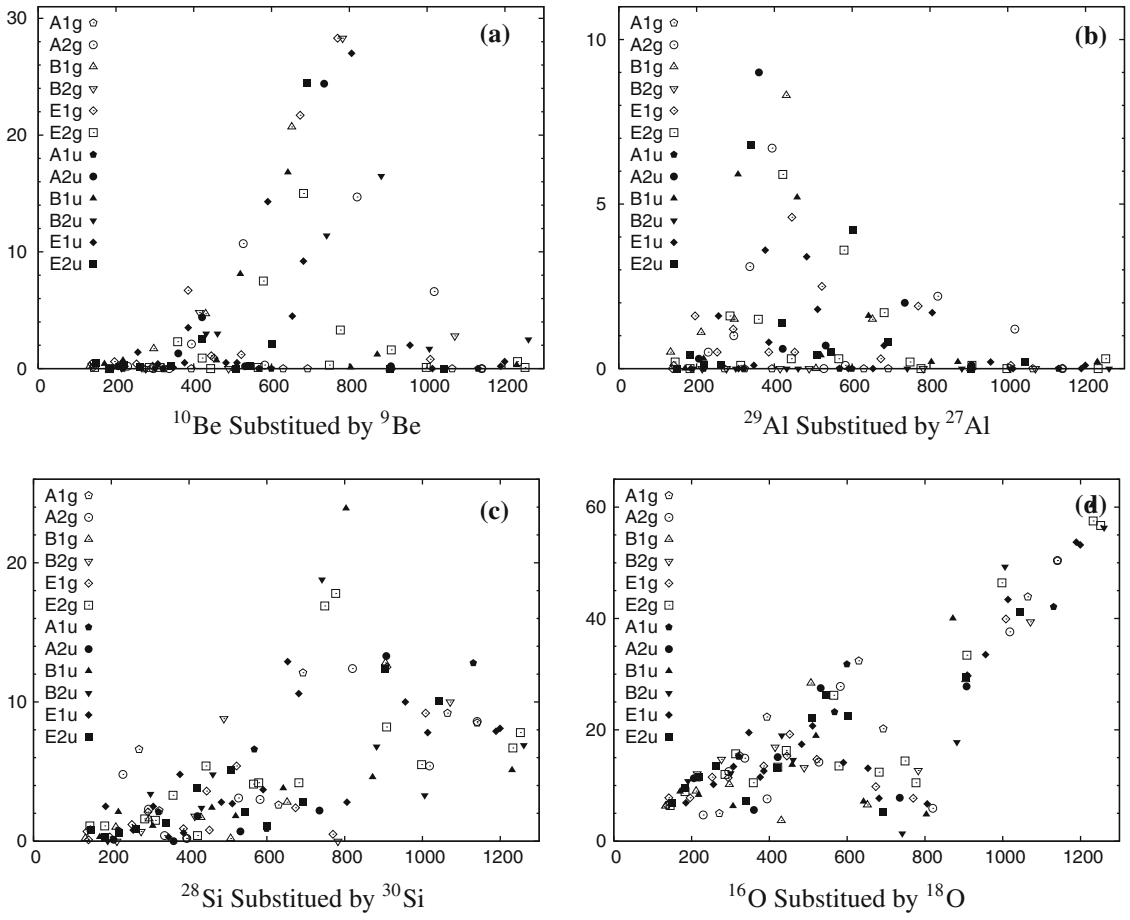

Fig. 2 Isotopic shifts (ordinate axis) versus frequencies of normal modes, relative to the four atomic species in the structure. Values in cm^{-1}

in the range $300 \div 460\,cm^{-1}$ (see Fig. 2b). The Raman active vibrations in which Al is involved are the modes 24, 51 and 61 of E_{1g} symmetry, and the modes 24, 47, 67 of E_{2g} symmetry, though the latter mode receives a relevant contribution by Be motion too. Only one IR active mode (i.e. 37 (A_{2u})) results mainly dominated by the Al motion. Si does participate to many normal modes in which Be is also involved, except those with the highest frequencies; this is well illustrated in Fig. 2c: vibrational modes having frequencies in the range between 400 and 1,000 cm^{-1} involve motion of either Be and Si; at frequencies higher than about 1,000 cm^{-1}, Si is dominating, with the exception of the silent modes 102, 105 and 114. Oxygens (O1 and O2) contribute to all of vibrations and the isotopic shifts increases roughly proportionally to the frequency of the modes; the contribution from oxygens appears to be less relevant (isotopic shift below 20 cm^{-1}) for modes with frequencies ranging from 600 to 800 cm^{-1}. In fact, in that spectral region, modes are more affected by the motion of Be and Si with isotopic shifts larger than 14 and 10 cm^{-1}, respectively.

At variance with respect to other silicates (e.g. forsterite; Noel et al. 2006), no large gaps are observed in separating the stretching/bending from the rest of the spectrum. This is due to the structure of beryl where Si tetrahedra are connected by vertex sharing to form both the six-membered ring and the connection to the Be tetrahedra. In fact, the gap between stretching and bending modes of the SiO_4 units is filled by the modes involving the motion of the Be atom and of the oxygen atom (O2) connecting Si and Be tetrahedra.

The graphical representation is perhaps the most useful tool for understanding the nature of the atomic motion involved in each vibrational mode; the reader is therefore referred to the CRYSTAL web site[2], where the animation of the normal modes has been provided for the case of beryl. We limit here to the discussion of some particular cases.

On the basis of factor group analysis, as discussed for instance by Hagemann et al. (1990), all of the A_{1g} modes derives from the motions of the atoms in the

[2] http://www.crystal.unito.it/vibs/beryl

2FL1

sixfold rings of Si-centred tetrahedra (Si, O1 and O2), with no contribution from Al and Be. Graphical animations[2] show that mode at 272 cm^{-1} (line 22 in Table 6) corresponds to anti-phase rotations around [001] of the two Si_6O_{18} rings stacked along the same axis; the motion of the O2 atoms causes deformations of the Be and Al-centred polyhedra. The mode at 324 cm^{-1} (line 33) is a *breathing mode* of the rings mainly due to bending of the Si–O1–Si angle, as O1 moves in the *XY* plane along the bisector of the Si–O1–Si angle. The mode at 395 cm^{-1} (line 43), is also a *breathing mode*, this time due to bending of the angles in Si, Be and Al-centred polyhedra. The mode at 630 cm^{-1}, (line 72) is essentially a bending mode involving the O2–Be–O2 and O2–Al–O2 angles; the O2 motion produces an anti-phase rotation of the rings. The mode at 692 cm^{-1} (line 80) is in some respect similar to that occurring at 395 cm^{-1}, but major bending deformations occurs in the Si-centred tetrahedra only. The mode at 1,065 cm^{-1} (line 104) is mainly an Si–O2 stretching mode coupled with O2–Al–O2 and O2–Be–O2 angles deformations. The mode at 1,132 cm^{-1} (line 108) appears to be a Si–O1 asymmetric stretching mode; the motion of the Si and O1 atoms is entirely confined in the *XY* plane and no deformation of Be and Al-centred polyhedra is involved.

Kim et al. (1995) attempted to establish the nature of the atomic motions, for all the experimentally observed modes, by looking at the eigenvectors of a dynamical matrix evaluated from a model potential parametrized to reproduce the *assumed* fundamental observed frequencies; the agreement with our assignements is however not fully satisfactory, since some of their assignements differs significantly from our owns.

Conclusion

An ab initio quantum-mechanical calculation of the vibrational spectrum of beryl, at the zone-centre has been performed. In general, the calculated Raman and IR frequencies are in excellent agreement with the experimental data obtained by different Authors. Some problems of leakage, overtone and combination bands are identified, in the available experimental data sets, as the reasons of a few discrepancies observed between our calculation and the experiments. The method used for the calculation proved to be more satisfactory than other essentially classical and empirical methods, based on model potentials, parametrized to fit the observed vibrational frequencies. The calculation provides the frequencies of both the active (Raman and IR) and inactive (*silent*) fundamental vibrational modes, which are essential for the *statistical* determination of many thermodymical properties; moreover, the nature of the atomic motion, involved in each normal mode, can definitely be established by using several tools provided for the analysis of the eigenvectors of the dynamical matrix.

Acknowledgments This work was supported by Project ''Phase transitions and order-disorder processes in minerals'' (MIUR, Roma). Dr. Y. Noel thanks the Centre Informatique National de l'Enseignement Supérieur (CINES), for its support.

References

Adams DM, Gardner IR (1974) Single-crystal vibrational spectra of beryl and dioptase. J Chem Soc Dalton Trans 1502–1505

Aines RD, Rossman GR (1984) The high-temperature behavior of water and carbon dioxide in cordierite and beryl. Am Mineral 69:319–327

Artioli G, Rinaldi R, Ståhl K, Zanazzi PF (1993) Structure refinements of beryl by single-crystal neutron and X-ray diffraction. Am Mineral 78:762–768

Aurisicchio C, Fioravanti G, Grubessi O, Zanazzi PF (1988) Reappraisal of the crystal chemistry of beryl. Am Mineral 73:826–837

Baranek P, Zicovich-Wilson C, Roetti C, Orlando R, Dovesi R (2001) Well localized crystalline orbitals obtained from Bloch functions: the case of $KNbO_3$. Phys Rev B64:125102

Binkley, Pople JA (1977) Self-consistent molecular orbital methods. XIX. Split-valence Gaussian-type basis sets for beryllium. J Chem Phys 66:879–880

Born M, Huang K (1954) Dynamical theory of crystal lattices. Oxford University Press, Oxford

Charoy B, de Donato P, Barres O, Pinto-Coelho C (1996) Channel occupancy in an alkali-poor beryl from Serra Branca (Goias, Brazil): spectroscopic characterization. Am Mineral 81:395–403

Civalleri B, D'Arco Ph, Orlando R, Saunders VR, Dovesi R (2001) Hartree-Fock geometry optimisation of periodic systems with the CRYSTAL code. Chem Phys Lett 348:131–138

Deer WA, Howie RA, Zussman J (1992) An introduction to the rock forming minerals. Longman Group, England, pp 116–121

Doll K, Saunders VR, Harrison NM (2001) Analytical Hartree-Fock gradients for periodic systems. Int J Quantum Chem 82:1–13

Ferraris G, Prencipe M, Rossi P (1998) Stoppaniite, a new member of the beryl group: crystal structure and crystal-chemical implications. Eur J Mineral 10:491–496

Gatta GD, Nestola F, Bromiley GD, Mattauch S (2006) The real topological configuration of the extra-framework content in alkali-poor beryl: a multi-methodological study. Am Mineral 91:29–34

Gervais F, Piriou B, Cabannes F (1972) Anharmonicity of infrared vibration modes in beryl. Phys Status Solidi 51:701–712

Hagemann H, Lucken A, Bill H, Gysler-Sanz J, Stalder HA (1990) Polarized Raman spectra of beryl and bazzite. Phys Chem Miner 17:395–401

Hawthorne FC, Černý P (1977) The alkali-metal positions in Cs–Li beryl. Can Mineral 15:414–421

Hawthorne FC, Waychunas GA (1988) Spectrum-fitting methods. In: Hawthorne FC (ed) Spectroscopic methods in mineralogy and geology. Reviews In Mineralogy 18:99–159. Reviews in Mineralogy, Mineralogical Society of America, Washington DC

Hofmeister AM, Hoering TC, Virgo D (1987) Vibrational spectroscopy of beryllium aluminosilicates: heat capacity calculations from band assignments. Phys Chem Miner 14:205–224

Kim CC, Bell MI, McKeown DA (1995) Vibrational analysis of beryl ($Be_3Al_2Si_6O_{18}$) and its constituent ring (Si_6O_{18}). Physica B 205:193–208

Koch W, Holthausen MC (2000) A chemist's guide to density functional theory. Wiley-VCH Verlag GmbH, Weinheim

Kolesov BA, Geiger CA (2000) The orientation and vibrational states of H_2O in synthetic alkali-free beryl. Phys Chem Miner 27:557–564

Mashkovtsev RI, Stoyanov ES, Thomas VG (2004) State of molecules and ions in the structural channels of synthetic beryl with an ammonium impurity. J Struct Chem 45:56–63

McMillan PF, Hofmeister AM (1988) Infrared and Raman Spectroscopy. In: Hawthorne FC (ed) Spectroscopic methods in mineralogy and geology. Reviews In Mineralogy 18:99–159. Reviews in Mineralogy, Mineralogical Society of America, Washington DC

Monkhrost HJ, Pack JD (1976) Special points for Brillouin-zone integration. Phys Rev B 8:5188–5192

Montanari B, Civalleri B, Zicovich-Wilson CM, Dovesi R (2006) Influence of the Exchange-correlation functional in all-electron calculations of the vibrational frequencies of corundum (α-Al_2O_3). Int J Quantum Chem 106:1703–1714

Nada R, Nicholas JB, McCarthy MI, Hess AC (1996) Basis sets for ab initio periodic Hartree-Fock studies of zeolite/adsorbate interactions: He, Ne, and Ar in silica sodalite. Int J Quantum Chem 60:809–820

Noel Y, Zicovich-Wilson C, Civalleri B, D'Arco Ph, Dovesi R (2002): Polarization properties of ZnO and BeO: An *ab initio* study through the Berry phase and Wannier functions approaches. Phys Rev B 65:014111

Noel Y, Catti M, D'Arco Ph, Dovesi R (2006) The vibrational frequencies of forsterite Mg_2SiO_4; an all-electron *ab initio* study with the CRYSTAL code. Phys Chem Miner 33:383–393

Orlando R, Torres J, Pascale F, Ugliengo P, Zicovich-Wilson CM, Dovesi R (2005) Vibrational spectrum of katoite $Ca_3Al_2[(OH)_4]_3$: a periodic ab initio study. J Phys Chem B 110:692–710

Pascale F, Tosoni S, Zicovich-Wilson CM, Ugliengo P, Orlando R, Dovesi R (2004a) Vibrational spectrum of brucite, $Mg(OH)_2$: a periodic ab initio quantum mechanical calculation including OH anharmonicity. Chem Phys Lett 396:4–6

Pascale F, Zicovich-Wilson CM, Gejo FL, Civalleri B, Orlando R, Dovesi R (2004b) The calculation of the vibrational frequencies of crystalline compounds and its implementation in the CRYSTAL code. J Comput Chem 25:888–897

Pascale F, Zicovich-Wilson CM, Orlando R, Roetti C, Ugliengo P, Dovesi R (2005a) Vibration frequencies of $Mg_3Al_2Si_3O_{12}$ pyrope. An ab initio study with the CRYSTAL code. J Phys Chem B 109:6146–6152

Pascale F, Catti M, Damin A, Orlando R, Saunders VR, Dovesi R (2005b) Vibration frequencies of $Ca_3Fe_2Si_3O_{12}$ andradite: an ab *ab initio* study with the crystal code. J Phys Chem B 109:18522–18527

Pilati T, Demartin F, Gramaccioli GM (1997) Lattice-dynamical evaluation of thermodynamic properties and atomic displacement parameters for beryl using a transferable empirical force field. Am Mineral 82:1054–1062

Pisani C, Dovesi R, Roetti C (1988) Hartree-Fock ab-initio treatment of crystalline systems. Lecture notes in chemistry, vol 48. Springer, Berlin Heidelberg New York

Prencipe M (2002) Ab initio Hartree-Fock study and charge density analysis of beryl ($Al_4Be_6Si_{12}O_{36}$). Phys Chem Miner 29:552–561

Prencipe M, Nestola F (2005) Quantum-mechanical modeling of minerals at high pressure. The role of the Hamiltonian in a case study: the beryl ($Al_4Be_6Si_{12}O_{36}$). Phys Chem Miner 32:471–479

Prencipe M, Pascale F, Zicovich-Wilson CM, Saunders VR, Orlando R, Dovesi R (2004) The vibrational spectrum of calcite (CaCO3): an ab initio quantum-mechanical calculation. Phys Chem Miner 31:559–564

Saunders VR, Dovesi R, Roetti C, Orlando R, Zicovich-Wilson CM, Harrison NM, Doll K, Civalleri B, Bush LJ, D'Arco Ph, Llunell M (2003) CRYSTAL2003 user's manual. University of Torino, Torino

Tosoni S, Pascale F, Ugliengo P, Orlando R, Saunders VR, Dovesi R (2005) Quantum mechanical calculation of the OH vibrational frequency in crystalline solids. Mol Phys 103:2549–2558

Ugliengo P, Pascale F, Merawa M, Labéguerie P, Tosoni S, Dovesi R (2004) Infrared spectra of hydrogen-bonded ionic crystals: ab initio study of $Mg(OH)_2$ and β-$Be(OH)_2$. J Phys Chem B 108:13632–13637

Umari P, Pasquarello A, Dal Corso A (2001) Raman scattering intensities in alpha-quartz: a first-principles investigation. Phys Rev B 63:094305

Wood DL, Nassau K (1967) Infrared spectra of foreign molecules in beryl. J Chem Phys 47:2220–2228

Wood DL, Nassau K (1968) The characterization of beryl and emerald by visible and infrared absorption spectroscopy. Am Mineral 53:777–800

Zicovich-Wilson CM, Dovesi R, Saunders VR (2001) A general method to obtain well localized Wannier functions for composite energy bands in linear combination of atomic orbital periodic calculations. J Chem Phys 115:9708–9719

Zicovich-Wilson CM, Bert A, Roetti R, Dovesi R, Saunders VR (2002) Characterization of the electronic structure of crystalline compounds through their localized Wannier functions. J Chem Phys 116:1120–1127

Zicovich-Wilson CM, Pascale F, Roetti C, Saunders VR, Orlando R, Dovesi R (2004) Calculation of vibration frequencies of alpha-quartz: the effect of hamiltonian and basis set. J Comput Chem 25:1873–1881